Switching Algorithms for the Dual Inverter fed Open-end Winding Induction Motor Drive for 3-level Voltage Space Phasor Generation

S. Srinivas[1] and V.T. Somasekhar[2]

Abstract – An open-end winding induction motor, fed by two 2-level inverters connected at either end produces space vector locations, identical to those of a conventional 3-level inverter. In this paper, two switching algorithms are proposed to implement space vector PWM for the dual inverter scheme. The proposed algorithms do not employ any look-up tables. The time consuming task of sector identification is altogether avoided in both these algorithms. The proposed algorithms employ only the instantaneous reference phase voltages for the implementation of the space vector PWM. An equal switching duty for both the inverters is also ensured with one of the proposed PWM strategies. Also, it is observed that the zero-sequence voltage in motor phases is significantly reduced with the proposed PWM strategies.

Keywords - Open-end winding induction motor drive, dual-inverter system, V/f control, space vector modulation

I. INTRODUCTION

Three-level inversion has been extensively researched in the past and several circuit topologies were suggested. Of these topologies, the neutral point clamped topology [1], the flying capacitor topology [2] and the H-bridge topology [3] have become popular. Recently, a circuit configuration to obtain three-level inversion by cascading two 2-level inverters has also been suggested [7].

Stemmler's pioneering work has shown that three-level inversion can be achieved by the open-end winding connection of an induction motor with two two-level inverters feeding the motor from either end [4]. In this work [4], sine-triangular modulation technique is employed for the control of inverters. Various derivatives of this power circuit and/or the associated PWM schemes are also reported in the recent past [6]-[14]. The inverters may be controlled with space vector modulation technique as it improves the DC-bus utilization compared to the sine-triangle modulation technique. A space vector modulation technique for the open-end winding topology has been suggested in [6]. In this work [6], the implementation of space vector modulation requires sector identification, which is a time consuming task. Further, this switching scheme employs lookup tables, enhancing the memory requirement with a typical Digital implementation.

Digital ref: A070101141
[1,2]Department of Electrical Engineering, National Institute of Technology-Warangal. Andhra Pradesh, INDIA. Pin: 506 004.
email: srsrini@nitw.ac.in
The paper first received on 5 Oct 2006 and in revised form 24 April 2007.

In this paper, two space vector modulation techniques are suggested, which obviate the need for the sector identification. Also these PWM schemes do not employ any look-up table, thus reducing the memory requirement.

This section gives a general background and review of the paper or work done by other engineers in the field. It should be well supported by citations. Moreover, the citations are served as a guide for those who want to learn more about the field.

Fig.1 shows the basic open-end winding induction motor drive operated with a single power supply. The symbols v_{AO}, v_{BO} and v_{CO} denote the pole voltages of the inverter-1. Similarly, the symbols $v_{A'O}, v_{B'O}$ and $v_{C'O}$ denote the pole voltages of inverter-2. The space vector locations from individual inverters are shown in Fig.2. The numbers 1 to 8 denote the states assumed by inverter-1 and the numbers 1' through 8' denote the states assumed by inverter-2 (Fig.2).

Table-1 summarizes the switching state of the switching devices for both the inverters in all the states. In Table-1, a '+' indicates that the top switch in a leg of a given inverter is turned on and a '-' indicates that the bottom switch in a leg of a given inverter is turned on.

As each inverter is capable of assuming 8 states independently of the other, a total of 64 space vector combinations are possible with this circuit configuration. The space vector locations for all space vector combinations of the two inverters are shown in Fig.3. In Fig.3, |OA| represents the DC-link voltage of individual inverters, and is equal to $V_{dc}/2$ while |OG| represents the DC-link voltage of an equivalent single inverter drive, and is equal to V_{dc}.

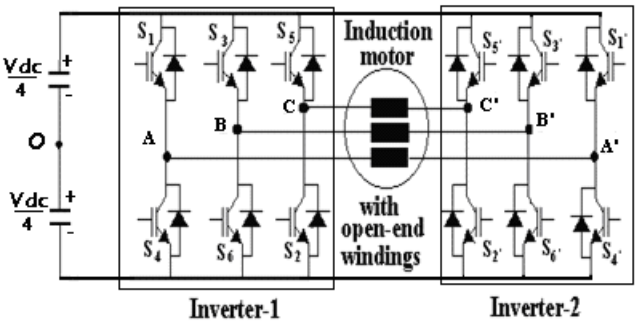

Fig.1: The primitive open-end winding induction motor drive

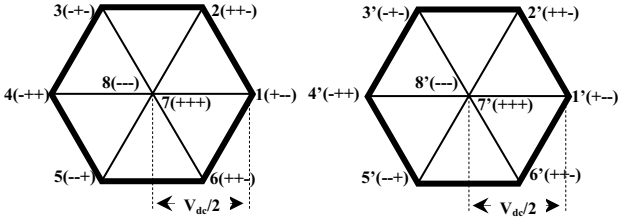

Fig. 2: Space vector locations of inverter-1 (Left) and inverter-2 (Right)

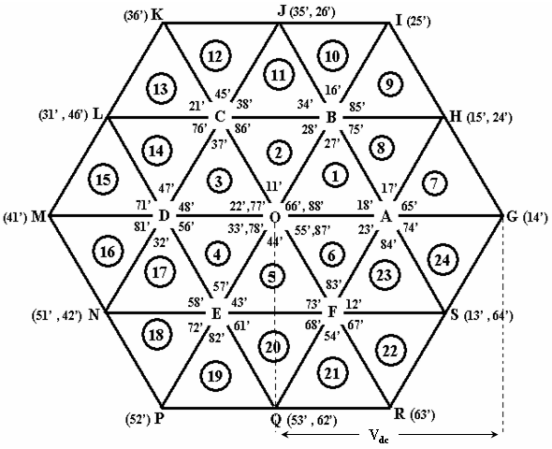

Fig.3: Resultant space vector combinations in the dual-inverter scheme

Table – 1: Switching states of the individual inverters

State of Inverter-1	Switches turned on	State of Inverter-2	Switches turned on
1 (+ - -)	S_6, S_1, S_2	1' (+ - -)	$S_{6'}$, $S_{1'}$, $S_{2'}$
2 (+ + -)	S_1, S_2, S_3	2' (+ + -)	$S_{1'}$, $S_{2'}$, $S_{3'}$
3 (- + -)	S_2, S_3, S_4	3' (- + -)	$S_{2'}$, $S_{3'}$, $S_{4'}$
4 (- + +)	S_3, S_4, S_5	4' (- + +)	$S_{3'}$, $S_{4'}$, $S_{5'}$
5 (- - +)	S_4, S_5, S_6	5' (- - +)	$S_{4'}$, $S_{5'}$, $S_{6'}$
6 (+ - +)	S_5, S_6, S_1	6' (+ - +)	$S_{5'}$, $S_{6'}$, $S_{1'}$
7 (+ + +)	S_1, S_3, S_5	7' (+ + +)	$S_{1'}$, $S_{3'}$, $S_{5'}$
8 (- - -)	S_2, S_4, S_6	8' (- - -)	$S_{2'}$, $S_{4'}$, $S_{6'}$

Fig.1 shows the basic open-end winding induction motor drive. It cannot be operated with a single power supply, due to the presence of zero-sequence voltages (common-mode voltages) [5], [6]. Consequently, a high zero-sequence current would flow through the motor phase windings, which is deleterious to the switching devices and the motor itself. To suppress the zero-sequence components in the motor phases, each inverter is operated with an isolated dc- power supply as shown in Fig.4. From the Fig.4, when isolated DC power supplies are used for individual inverters, the zero-sequence current cannot flow as it is denied a path. Consequently, the zero-sequence voltage appears across the points 'O' and 'O'". The zero-sequence voltage resulting from each of the 64 space vector combinations is reproduced in Table-2 from [6] to facilitate an easy reference.

In Fig.5, the vector **OT** represents the reference vector (also called the reference sample), with its tip situated in sector-7 (Fig.3). This vector is to be synthesized in the average sense by switching the space vector combinations situated in the closest proximity (the combinations situated at the vertices A, G and H in the present case) using the space vector modulation technique. In the work reported in reference [7], the reference vector **OT** is transformed to **OT'** in the core hexagon ABCDEF by using an appropriate coordinate transformation, which shifts the point A to point O. In the core hexagon, the switching timings of the active vectors **OA**, **OB** and the switching time of the null vector situated at **O** to synthesize the transformed reference vector **OT'** are evaluated. The switching algorithm described in reference [5] is employed to evaluate these timings. These timings are then employed to produce the actual reference vector **OT** situated in sector-7 by switching amongst the switching

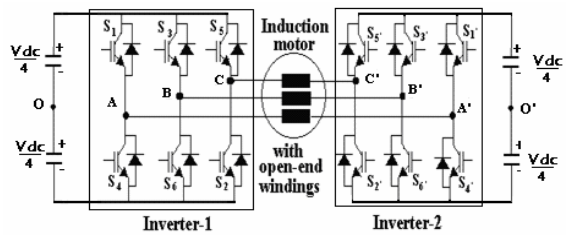

Fig. 4: The open-end winding induction motor drive with two isolated power supplies

Table – 2: Zero-sequence voltage contributions in the difference of the pole- voltages of individual inverters

$-V_{dc}/2$	$-V_{dc}/3$	$-V_{dc}/6$	0	$V_{dc}/6$	$V_{dc}/3$	$V_{dc}/2$
8-7'	8 – 4' 8 – 6' 8 – 2' 5 – 7' 3 –7' 1 – 7'	8 - 5 ' 8 - 3' 5 – 4', 3 – 4' 8 – 1', 5 – 6' 5 – 2', 3 – 6' 3 – 2', 4 – 7' 1 – 4', 1 – 6' 1 – 2', 6 – 7' 2 – 7'	8 - 8', 5 - 5', 5 - 3', 3 – 5', 3 – 3', 4 – 4', 5 – 1', 3 – 1', 4 – 6'. 4 – 2', 1 – 5', 1 – 3', 6 – 4', 2 – 4', 1 – 1', 6 – 6', 6 – 2', 2 – 6', 2 – 2', 7 – 7'	5 – 8', 3 - 8', 4 – 5', 4 – 3' 4 – 1', 1 – 8' 6 – 5', 6 – 3' 2 – 5', 2 – 3' 7 – 4', 6 – 1' 2 – 1', 7 – 6' 7 – 2'	4 – 8' 6 – 8' 2 – 8' 7 – 5' 7 – 3' 7 – 1'	7 – 8'

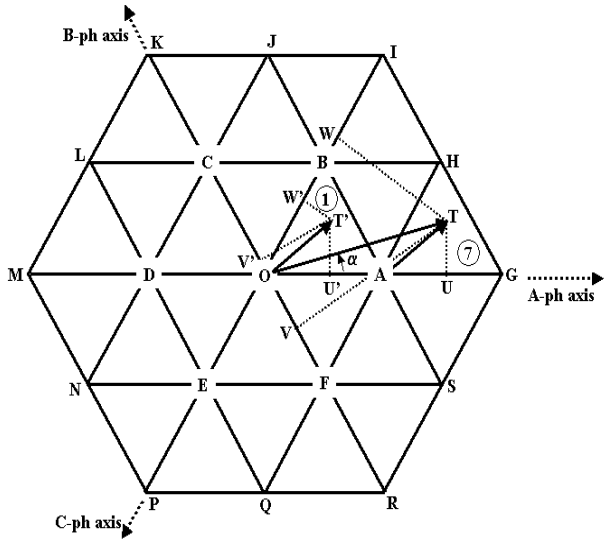

Fig.5: Resolution of the reference voltage space vector in the middle and outer sectors

combinations available at the vertices A, G and H. The latter step requires a lookup table in which the space vector combinations available at each space vector location are stored.

Thus, it is evident that with this switching algorithm, the controller negotiates a considerable computational burden primarily because of sector identification and coordinate transformation. Also, there is a need requirement for look-up tables, enhancing the memory requirement. Further, the zero-sequence voltage in the difference of the respective pole voltages of individual inverters (which is dropped across the points 'O' and 'O'' in Fig.4) is also high with this PWM scheme.

II. Proposed PWM strategies

The proposed PWM strategies are based on the following observations:

1. The resultant space vector locations in the dual-inverter scheme (Fig.3) are obtained by superposing the space vector locations resulting from inverter-2 (i.e. by superposing the center of the right hexagon, Fig.2) at each space vector location caused by inverter-1 (left hexagon, Fig.2). Alternatively, the space vector locations of the resulting dual inverter scheme may be obtained by superposing the center of the left hexagon at each of the space vector locations of the right hexagon.
2. Apart from the core hexagon ABCDEF centered around O, there exist six outer sub-hexagons namely OBHGSF, OCJIHA, ODLKJB, OENMLC, OFQPND and OASRQE centered around the points A, B, C, D, E and F respectively. For the rest of this paper, they are referred to as sub-hexagonal centers.
3. The space vector combinations at the vertices and at the center of a given sub-hexagon are obtained by clamping one inverter to a given state while the other inverter assumes all the eight states. For example, the space vector combinations at the vertices of the sub-hexagon OFSGHB (centered around the point 'A', Fig.3), are obtained by clamping inverter-1 to the state of 1(+--), while inverter-2 assumes the states 1' to 6' respectively. The space vector combinations at the sub-hexagonal center 'A' are given by the active vector to which inverter-1 is clamped (in this case to state-1) and the null vectors of inverter-2 (states 8' and 7', Table-1) respectively.
4. All the seven locations of a given sub-hexagonal center (i.e. six vertices and the corresponding sub-hexagonal center) show redundancy of space vector combinations. For the sub-hexagon OFSGHB, the space vector combinations for these seven locations may alternatively be obtained by clamping inverter-2 to state 4'(-++) while inverter-1 assumes all the eight states.
5. Of the 20 space vector combinations with a common-mode voltage contribution of zero, 8 are located at the origin O (Table-2, Fig.3). Therefore, any PWM strategy that makes a good use of these states is expected to cause a reduction in the zero-sequence voltages, in the difference of the pole-voltages of respective inverters.

The following PWM strategies are proposed in this paper:

- The Decoupled PWM strategy
- The Biasing inverter PWM strategy

III. The Decoupled PWM strategy

This PWM strategy is based on the fact that the reference voltage space vector V_{sr} can be synthesized with two equal and opposite components $V_{sr}/2$ and $-V_{sr}/2$, by subtracting the latter component from the former. It is also based on the observation that the effect of applying a vector with inverter-1 while inverter-2 assumes a null state is the same as that of applying the opposite vector with inverter-2 while inverter-1 assumes a null state. Figure 6 shows the method of this PWM strategy. It is worth noting that the phase axes of the motor viewed with reference to individual inverters are in phase opposition.

In Fig.6, the vector **OT** represents the actual reference voltage space vector that is to be synthesized from the dual-inverter system and is given by $V_{sr} \angle\alpha$. This vector is resolved into two equal and opposite components $\mathbf{OT_1}$ ($V_{sr}/2 \angle\alpha$) and $\mathbf{OT_2}$ ($V_{sr}/2 \angle 180^o + \alpha$). The vector $\mathbf{OT_1}$ is synthesized by inverter-1 in the average sense by switching amongst the states (8-1-2-7) while the vector $\mathbf{OT_2}$ is reconstructed by inverter-2 in the average sense by switching amongst the states (8'-5'-4'-7').

The basic switching algorithm described in reference [5] for the classical case of a 2-level inverter feeding an ordinary induction motor is extended for the dual-inverter system to compute the switching timings for individual inverters.

These two strategies are described in detail in the following sub-sections.

This algorithm [5] uses only the instantaneous phase reference voltages and is based on the concept of 'effective time'. The effective time is defined as the time

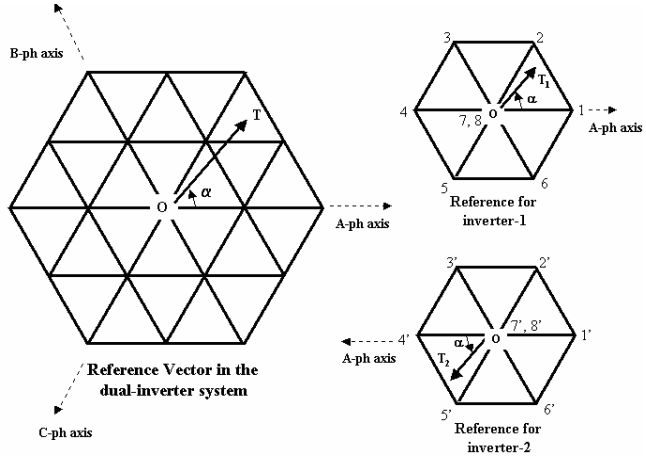

Fig.6: The decoupled PWM strategy

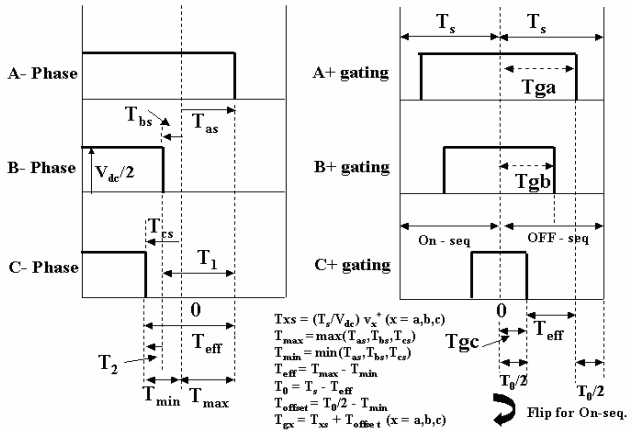

Fig.7: Generation of switching sequence with algorithm reported in reference [8]

for which the inverter supplies power to the motor in a given sampling time period and is denoted as T_{eff}. The sampling time period is denoted as T_s. The instantaneous phase reference voltages are obtained by projecting the tip of the reference vector V_{sr} on to the respective phase axes and multiplying the values of these projections with a factor of (2/3). These instantaneous phase reference voltages are denoted as v_a^*, v_b^* and v_c^*. This algorithm accomplishes the automatic generation of the gating pulses for the individual switching devices while placing the effective time exactly at the center of a given sampling time period. The symbols T_{ga}, T_{gb} and T_{gc} respectively denote the time duration for which a given motor phase is connected to the positive rail of the input DC power supply of the inverter in the given sampling time period Ts. The timings T_{ga}, T_{gb} and T_{gc} are termed as the phase switching times. The procedure to generate the gating pulses for the individual devices using this algorithm in sector-1 is pictorially depicted in Fig.7. A similar procedure is adopted for all the other sectors.

In the context of a dual inverter drive, there exist two sets of phase switching times, one for each inverter. The timings T_{ga}, T_{gb} and T_{gc} correspond to inverter-1 while the timings $T_{ga}^{'}$, $T_{gb}^{'}$ and $T_{gc}^{'}$ correspond to inverter-2. The instantaneous reference phase voltages v_a^*, v_b^* and v_c^* correspond to the actual reference space vector V_{sr} of the dual-inverter system. As individual inverters operate with the references $V_{sr}/2$ and $-V_{sr}/2$ respectively, it follows that the corresponding phase references are given by, $v_a^*/2$, $v_b^*/2$ and $v_c^*/2$ for inverter-1 and $-v_a^*/2$, $-v_b^*/2$ and $-v_c^*/2$ for inverter-2. These references are then employed to determine the phase switching timings of each inverter using the aforementioned switching algorithm [8]. It can be shown mathematically that the phase switching times of the inverters are related by (the proof of this result is presented in appendix-A):

$$T_{ga}^{'} = T_s - T_{ga} \; ; \; T_{gb}^{'} = T_s - T_{gb}^{'} \; ; \; T_{gc}^{'} = T_s - T_{gc}$$

Thus, the phase switching timings need not be exclusively computed for inverter-2. Both inverters are operated with the same sequence so that the null vector combinations are 88' and 77'. From table-1, it may be noted that these two combinations result in the zero-sequence voltage that is zero. If one inverter is operated with on-sequence and the other with off-sequence, the null vector combinations would be 87' or 78'. From table-2 it is evident that the zero-sequence voltage of the difference of the pole-voltages is maximum for these two combinations. It is interesting to note that this zero-sequence voltage is much lesser with this algorithm than the lookup table approach used in [6]. This is because the combinations 87' and 78' are used extensively with that approach [6]. The merit of the decoupled control is that there is no computational burden on the controller and is therefore amenable to be used with slower controllers (processors) and possibly the reduced zero-sequence voltage in the difference of pole-voltages. However, in this approach, both inverters are to be switched.

IV. Experimental Verification for the Decoupled PWM Strategy

The performance of the dual-inverter scheme is first evaluated with simulation studies using MATLAB and the induction motor is operated with the V/f control scheme. The experiment is performed on a 1 H.P. open-end winding induction motor with V/f control and the gating signals to the dual-inverter are generated with TMS320F240 Digital Signal Processor. A fixed number of samples (48) are employed for the implementation of the space vector modulation per cycle in the entire range of operation. This means that the sampling time period is a variable quantity. In the present case, the number of samples used per cycle is 48. This means that the angular displacement between successive samples is 7.5^0 (360/48). Fig.8 shows a typical sample. This is the 4th sample from the beginning of the cycle and occurs at $\alpha = 22.5^0$ (Fig.6). The modulation index, denoted as 'm$_i$,' is given by V_{sr}/V_{dc}. It may be noted from Fig.8 that $T_{ga} + T_{ga}^{'} = T_s$ as mentioned earlier. Therefore, the phase timings for inverter-2 need not be evaluated separately. They are obtained simply by subtracting the timings of the corresponding phases from T_s.

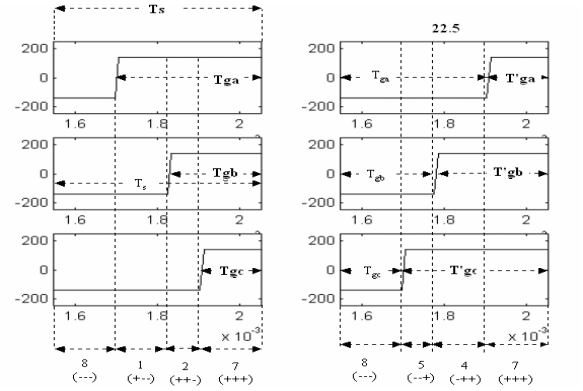

Fig.8: A typical sample with decoupled control

The top traces of Fig.9 show the gating signals of the top devices of the A-phase legs of the individual inverters for m_i = 0.4. The bottom trace of the same figure shows the difference of the two pole voltages, which contains a significant zero-sequence voltage. Fig.10 shows the simulated (left) and experimentally obtained (right) results of the pole voltages for phase-A of the inverter-1 and Fig.11 show the same for inverter-2 both for a modulation index of m_i = 0.4. Fig.12 shows the difference of these pole voltages and Fig.13 shows the simulated and experimentally obtained result of the actual motor phase voltage for m_i = 0.4. Of these, the latter waveform is obtained after the subtraction of the common-mode voltages from the difference of pole voltages shown in Fig.12. As isolated DC power supplies are employed in the present case, the zero-sequence voltage is dropped between the negative bus terminals of the individual inverters. Fig.14 shows the simulated and experimentally obtained results of the zero-sequence voltage. Figure 15 shows the experimentally obtained motor phase current at no-load for the same m_i of 0.4.

Figures 16 and 17 respectively shows the normalized harmonic spectra of the difference in pole voltages and actual motor phase voltage presented in Fig.12 and 13. It is seen from Fig.16 that the zero-sequence voltage in the difference of pole-voltages is significantly reduced compared with the strategy adopted in [7].

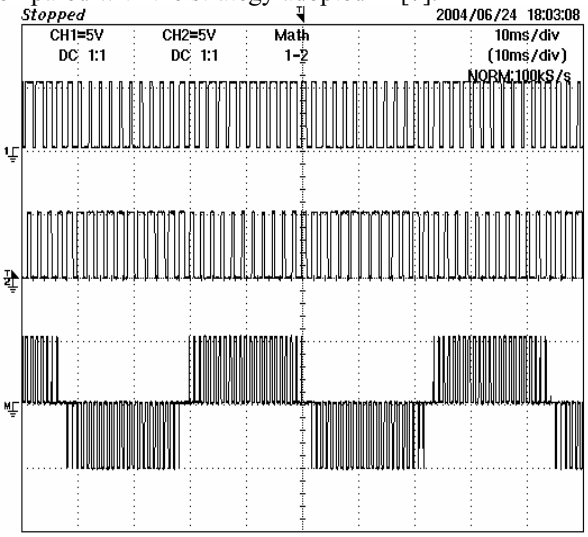

Fig.9: Gating signals and the difference of pole-voltages derived as the difference of two gate signals of top switch of the a-phase legs of the two inverters for m_i = 0.4

For example, the normalized third harmonic component is about 1.4 p.u. with the strategy adopted in [7], while it is only about 0.2 p.u. (Fig.16) with the decoupled control of the dual-inverter scheme for the same modulation index of mi=0.4. It may be noted from Fig.16 that, apart from the fundamental, the 47th and the 49th harmonics are dominant as the sampling frequency is 48 times the frequency of the fundamental component. The corresponding waveforms for a modulation index of m_i=0.7 are shown through Fig.18 to Fig.25.

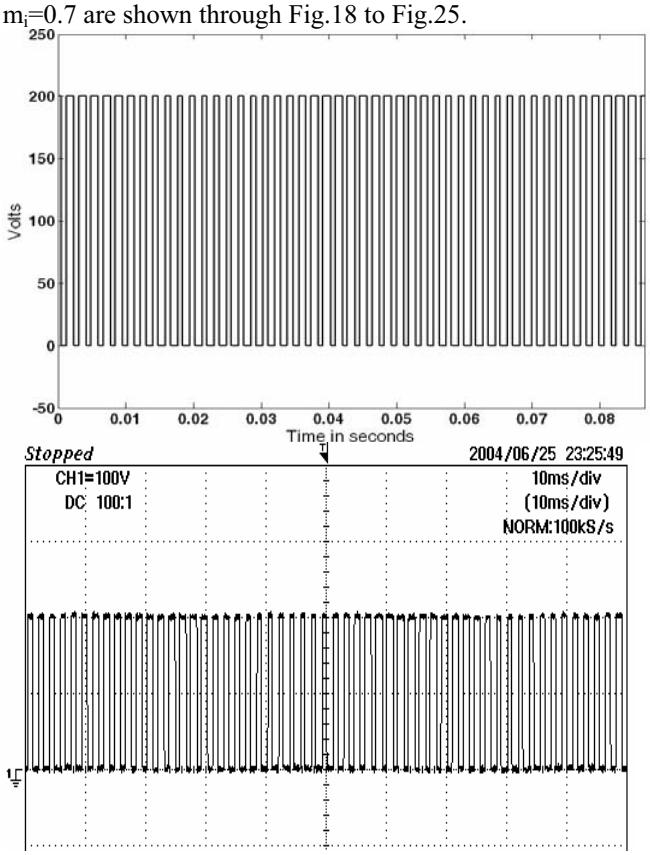

Fig.10: Simulated (top) & experimentally obtained result (bottom) of Pole voltage of inverter-1 for m_i = 0.4

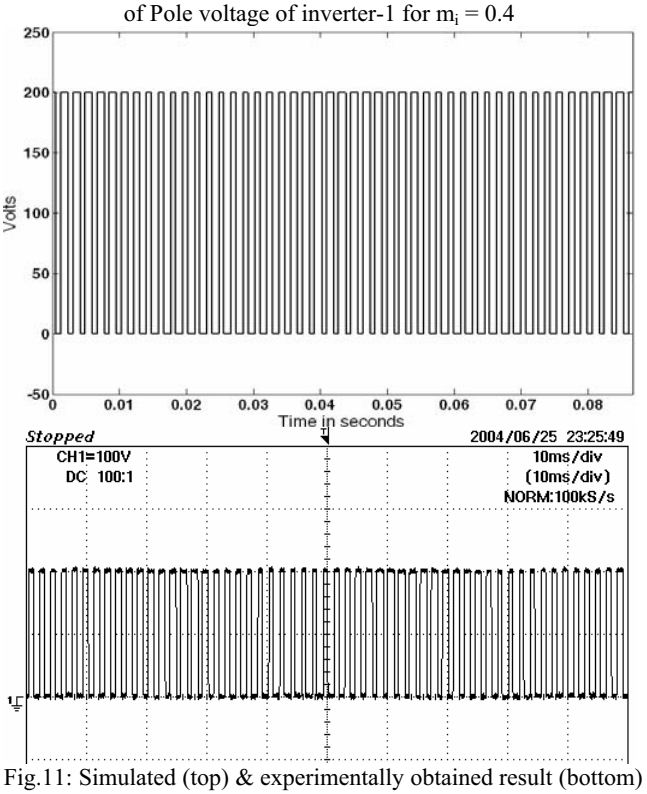

Fig.11: Simulated (top) & experimentally obtained result (bottom) of Pole voltage of inverter-2 for m_i = 0.4

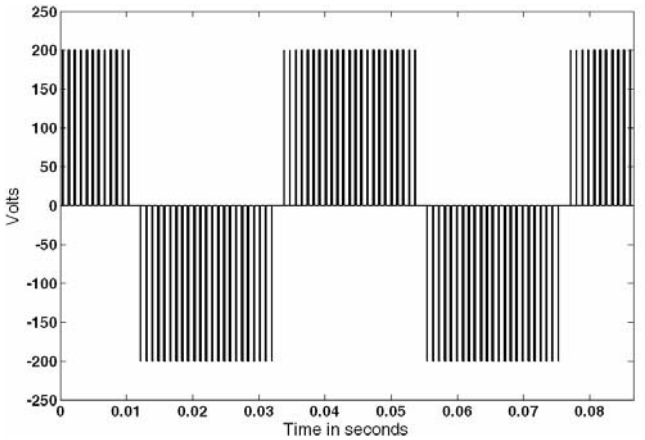

Fig.12: The difference of pole voltages of individual inverters for $m_i = 0.4$

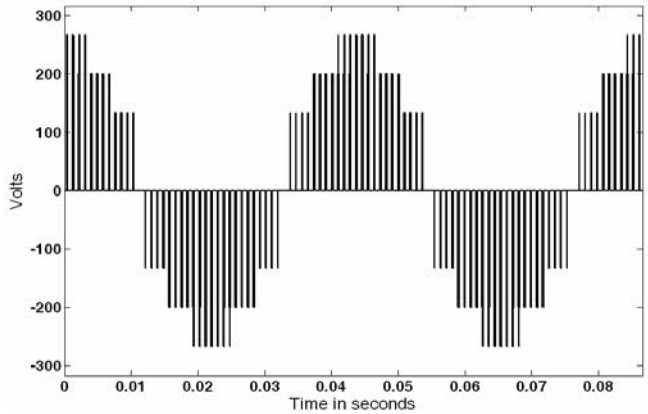

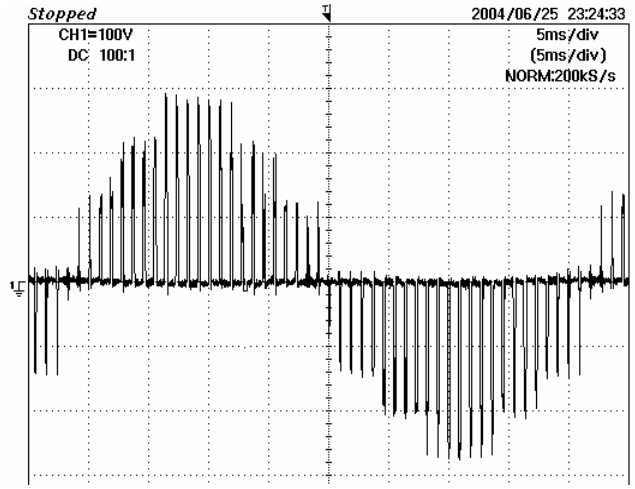

Fig.13: Simulated (top) & experimentally obtained result (bottom) of the actual motor phase voltage for $m_i = 0.4$

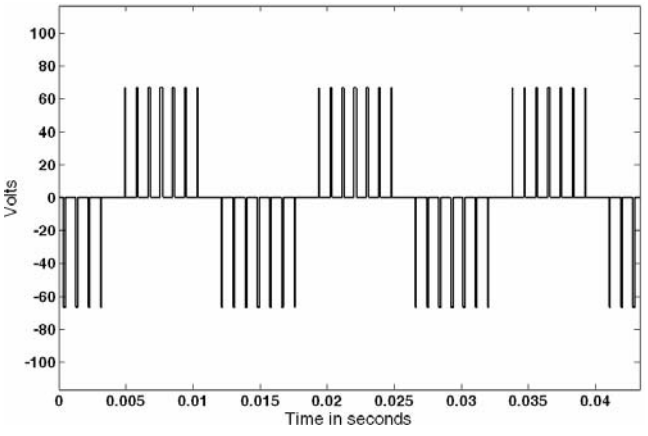

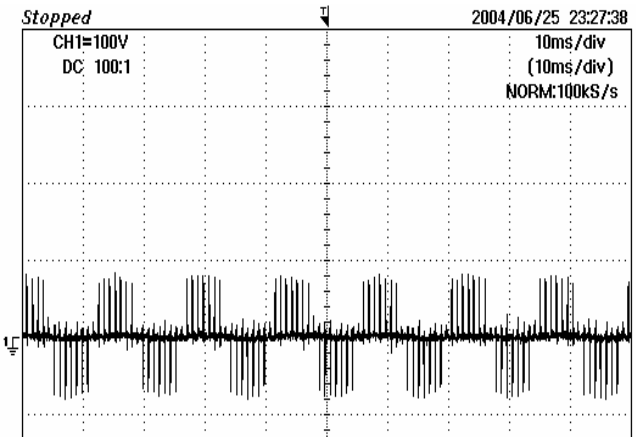

Fig.14: Simulated (top) & experimentally obtained result (bottom) of the common-mode voltage for $m_i = 0.4$

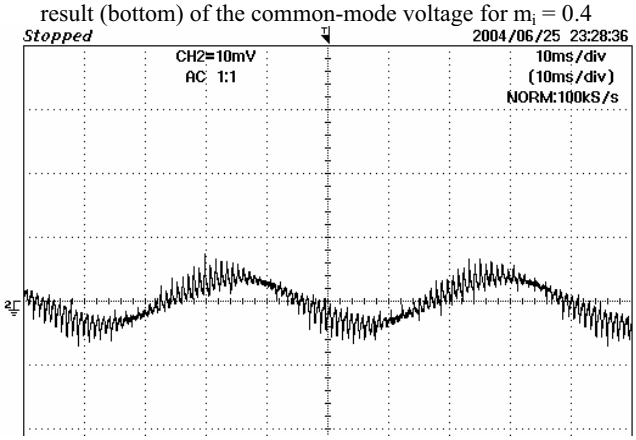

Fig.15: Experimentally obtained motor phase current at no-load for $m_i = 0.4$

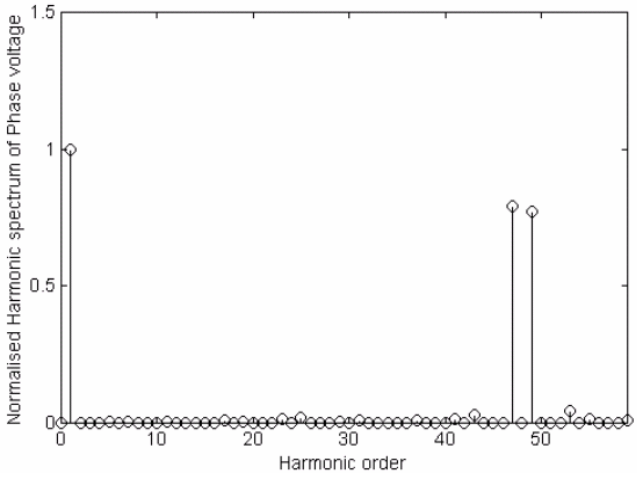

Fig.16: The normalized harmonic spectrum of the difference of pole voltages for $m_i = 0.4$

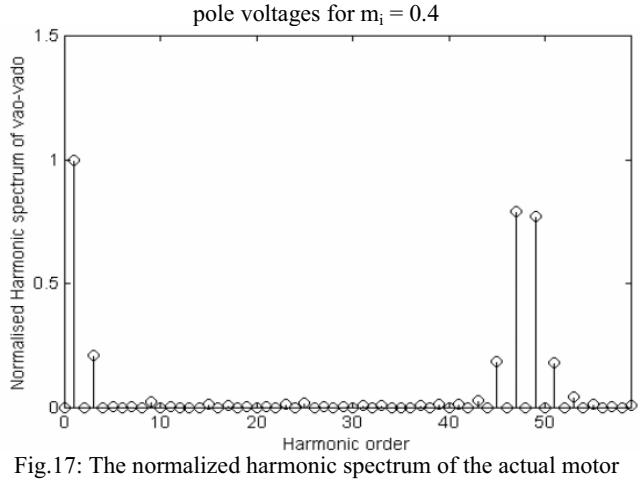

Fig.17: The normalized harmonic spectrum of the actual motor phase voltage for $m_i = 0.4$

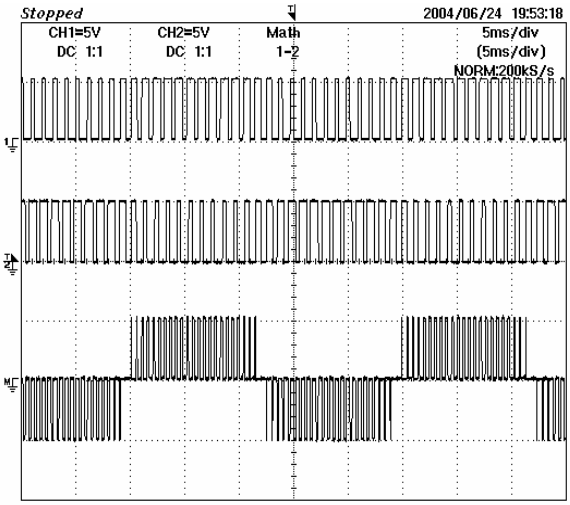

Fig.18: Gating signals and the difference of pole-voltages derived as the difference of two gate signals of top switch of the a-phase legs of the two inverters for $m_i = 0.7$

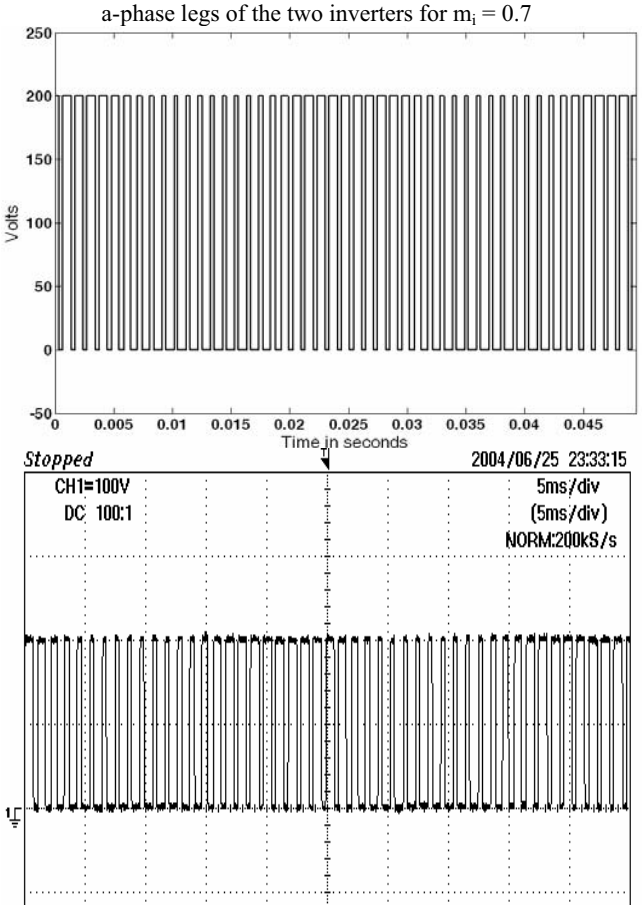

Fig.19: Simulated (top) & experimentally obtained result (bottom) of Pole voltage of inverter-1 for $m_i = 0.7$

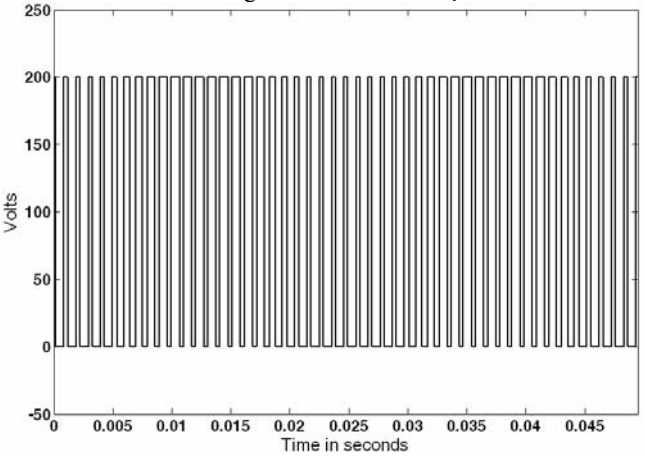

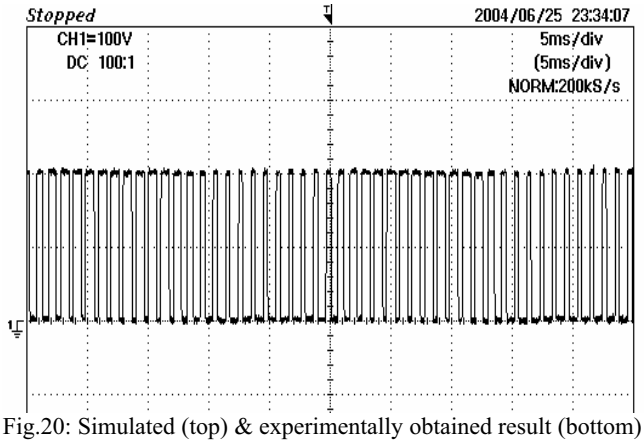

Fig.20: Simulated (top) & experimentally obtained result (bottom) of Pole voltage of inverter-2 for $m_i = 0.7$

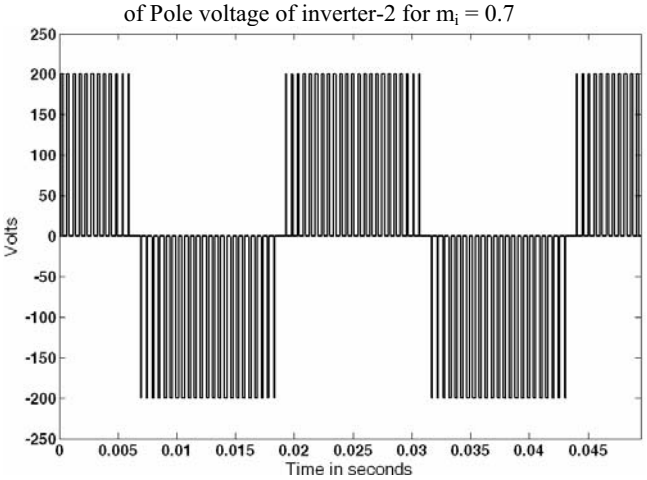

Fig.21: The difference of pole voltages of individual inverters for $m_i = 0.7$

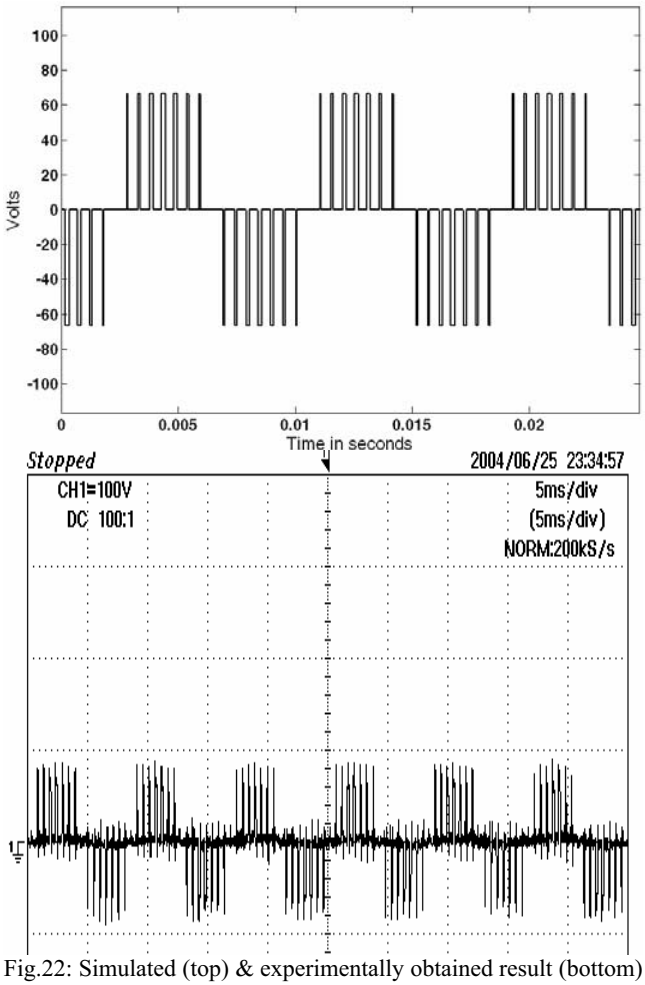

Fig.22: Simulated (top) & experimentally obtained result (bottom) of the common-mode voltage for $m_i = 0.7$

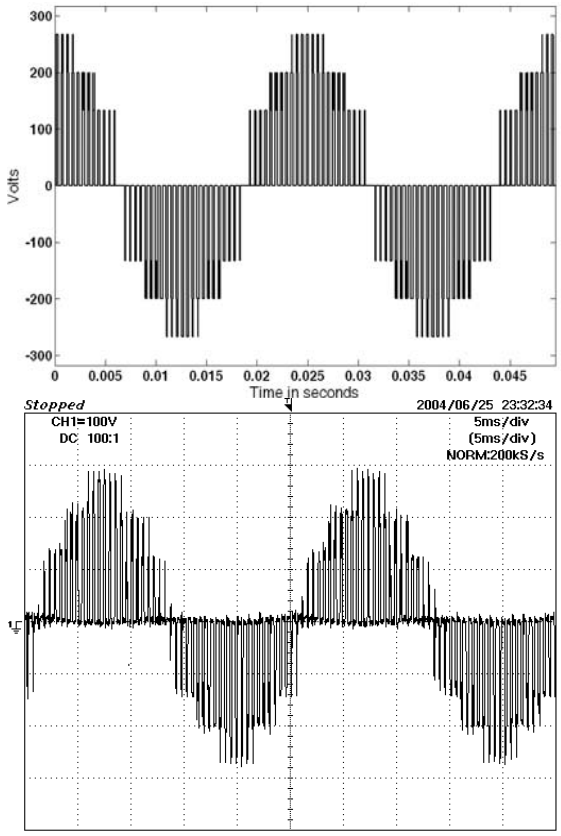

Fig.23: Simulated (top) & experimentally obtained result (bottom) of the actual motor phase voltage for $m_i = 0.7$

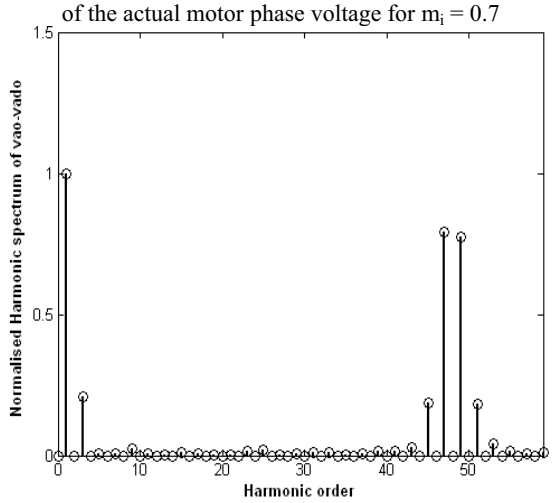

Fig. 24: Normalized harmonic spectrum of the difference of the pole voltages for $m_i = 0.7$

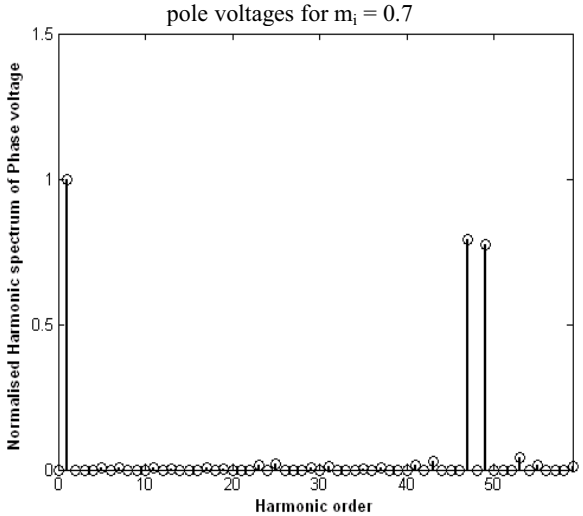

Fig. 25: Normalized harmonic spectrum of the motor phase voltage for $m_i = 0.7$.

V. The Biasing inverter PWM strategy

This PWM strategy is based on the observation that the space vector combinations at the vertices and the center of a given sub-hexagon are obtained by clamping one inverter with an active state, while the other inverter assumes all the eight states. Consequently, one inverter may be employed as the biasing inverter to realize the biasing vector and the other inverter may be switched around this biasing vector. Figure 26 shows the basic operating principle of this PWM strategy.

In Fig 26, **OT** represents the reference vector with its tip situated in sector-7. It is resolved into two components **OA** and **AT**. The vector **OA** may be output with inverter-1 with its state clamped at 1(+--, Table-1) throughout the sampling time interval. The vector **AT** is realized in the average sense by switching inverter-2 around the sub-hexagonal center, A. Alternatively, the biasing vector **OA** may be output with inverter-2 with its state clamped at 4'(-++, Table-1) throughout the sampling time interval. In that case, the switching vector **AT** is generated with inverter-1.

The instantaneous phase references denoted by, v_a^*, v_b^* and v_c^* corresponding to the reference vector **OT** are obtained by projecting its tip on to the respective phase axes and multiplying the values of these projections (OU, OV and OW, Fig.26) with a factor of (2/3). The symbols v_α^* and v_β^* respectively denote the components of **OT** on the α- and the β- axes (OU and OX, Fig.26). The modified instantaneous voltage phase references corresponding to the switching vector **AT** are denoted by, v_a , v_b and v_c are obtained by the following procedure:

1. The instantaneous phase references v_a^* , v_b^* and v_c^* corresponding to the reference vector **OT** are transformed into the corresponding equivalent two-phase system references v_α^* and v_β^* using the classical three phase to two phase transformation given by:

$$\begin{bmatrix} v_\alpha^* \\ v_\beta^* \end{bmatrix} = \begin{bmatrix} \frac{3}{2} & 0 & 0 \\ 0 & \frac{\sqrt{3}}{2} & -\frac{\sqrt{3}}{2} \end{bmatrix} \begin{bmatrix} v_a^* \\ v_b^* \\ v_c^* \end{bmatrix}$$

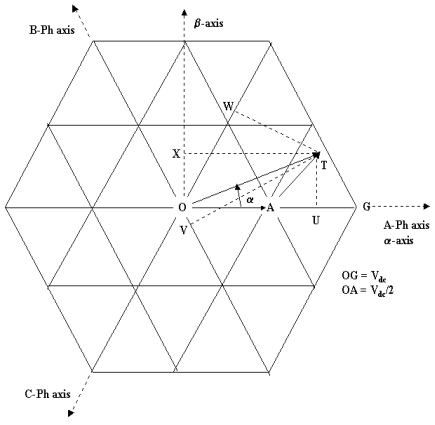

Fig.26: Principle of biasing inverter PWM strategy

2. The sub-hexagonal center situated nearest to the tip of the reference vector **OT** is then determined.

3. The coordinates of the nearest sub-hexagonal center in the $v_\alpha - v_\beta$ plane (the point 'A' in this example, Fig.26), denoted as $v_{\alpha,nshc}$ and $v_{\beta,nshc}$ are known for all the six sub-hexagonal centers. For example, the coordinates of the point 'A' in the $v_\alpha - v_\beta$ plane are given by (Vdc/2,0).

4. Since the vector **OA** is output by the biasing inverter, the coordinates of the switching vector (**AT** in the present case) denoted as $V_{\alpha,sw}$ and $V_{\beta,sw}$ are given by:
$V_{\alpha,sw} = v_\alpha^* - v_{\alpha,nshc}$ and $V_{\beta,sw} = v_\beta^* - v_{\beta,nshc}$

5. The modified reference phase voltages v_a, v_b and v_c for the switching inverter are then obtained by transforming $V_{\alpha,sw}$, $V_{\beta,sw}$ into the corresponding three phase variables by using the classical two phase – three phase transformation given by:

$$\begin{bmatrix} v_a \\ v_b \\ v_c \end{bmatrix} = \begin{bmatrix} 2/3 & 0 \\ -1/3 & 1/\sqrt{3} \\ -1/3 & -1/\sqrt{3} \end{bmatrix} \begin{bmatrix} V_{\alpha,sw} \\ V_{\beta,sw} \end{bmatrix}$$

6. If inverter-2 is employed as the biasing inverter, the modified references are used directly to generate the switching vector **AT** with inverter-1. On the other hand, if inverter-1 is used as the biasing inverter, it is obvious that the modified references must be negated to generate the switching vector **AT** with inverter-2.

The principal advantage with this PWM strategy is that the inverter switching is significantly reduced as one inverter switches only six times, while the other switches for 48 times. With decoupled control both inverters are switched in all the 48 samples.

It is important to note that the most important part of this algorithm is to find the nearest sub-hexagonal center to the tip of the reference vector **OT** (Fig.26). Fig.27 and Fig.28 explain the method to determine the same. In the discussion to follow, the symbol 'θ' denotes the angle subtended by the tip of the reference voltage space vector with respect to an instant where the instantaneous value of the A-phase reference voltage is zero. Fig.27 shows various values of 'θ' corresponding to the positive and the negative zero crossings of the reference phase voltages in the $V_\alpha - V_\beta$ plane. From Fig.27, it may be noted that if 0º ≤ θ ≤ 60º, the tip of V_{sr} is situated in the quadrangle OSRQ. It may also be seen that 'F' is the nearest sub-hexagonal center for this condition. Should the tip of the reference vector be situated within the quadrangle OSGH, 'A' is the nearest sub-hexagonal center to it. Similar observations may be made for the rest of the sub-hexagonal centers. It is desirable to identify the nearest sub-hexagonal center directly from the instantaneous phase references without having to evaluate V_{sr} and there by the value of 'θ', as it would be very time consuming.

The instantaneous phase reference voltages v_a^*, v_b^* and v_c^* (solid lines) normalized w.r.t V_{sr} and their respective negations (dotted lines) are shown in Fig.28. From Fig.28 it may be noted that v_a^* is the most positive quantity amongst these six quantities when 60º ≤ θ ≤ 120 º and 'A' is the nearest sub-hexagonal center as recognized by Fig.27. Similarly $-v_a^*$ is the most positive quantity amongst these six when 240º ≤ θ ≤ 300º and 'D' is the nearest sub-hexagonal center. Figure 27 also reinforces this fact. Thus, it is clear that by finding the maximum value amongst these six quantities, one can determine the nearest sub-hexagonal center.

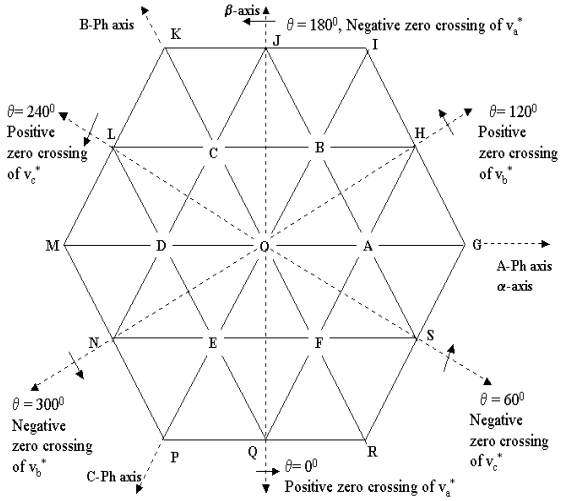

Fig.27: Zero crossing of the instantaneous phase voltages corresponding to the reference voltage space vector

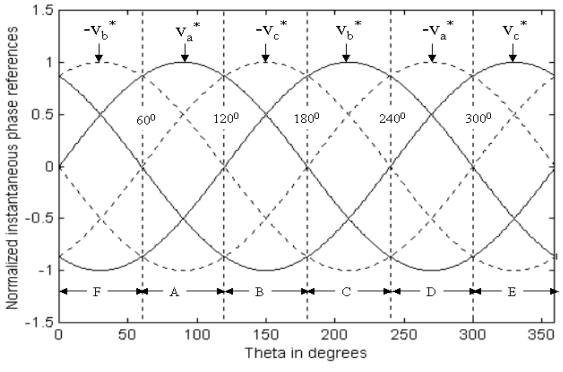

Fig.28: Recognition of the nearest sub-hexagonal center with instantaneous reference quantities

VI. Experimental Verification for Biasing inverter PWM strategy:

The top traces of Fig.29 show the gating signals of the top devices of the A-phase legs of the individual inverters for mi = 0.4. In this case, the samples of the reference vector always lie within the core hexagon ABCDEF. The bottom trace of the same figure shows the difference of the two pole voltages. Figures 30 and 31 show the respective pole voltages (both simulated & experimental results) of the

individual inverters with this PWM strategy. From these two figures, it is evident that the switching of inverter-1 is drastically reduced as it is made to operate as the biasing inverter for all samples in a cycle. However, the switching of inverter-2 remains unaltered as it is used as the switching inverter for all the samples in a cycle. Figure 32 shows the difference of the pole voltages, while Fig.33 shows the actual motor phase voltage (obtained after the subtraction of the zero-sequence voltage from the waveform shown in Fig.34). In this case, the phase voltage waveform is similar to the one obtained by a conventional two-level inverter. However, the switching ripple with the open-end winding configuration is much lesser compared to the one obtained with a two-level inverter. This is because; the space vector l9 locations situated at the closest proximity are switched with open-end winding drive. Specifically, if the sample is situated in sector-1, the vertices 'O', 'A' and 'B' are switched, unlike in a two-level inverter, where the location 'O', 'G' and 'I' are switched to construct the same sample (Fig.3). Fig.34 shows the simulated and experimentally obtained results of the zero-sequence voltage. Figures 35 and 36 respectively show the harmonic spectra of the difference in pole voltages (shown in Fig.32) and the actual motor phase voltage (shown in Fig.34). Figure 37 shows the experimentally obtained motor phase current at no-load for the same m_i of 0.4.

The corresponding waveforms for a modulation index of m_i=0.7 are shown through Fig.38 to Fig.45. In this case, the tip of the reference vector traverses through the outer sectors i.e. 7 to 24. It is also evident that the phase voltage waveform is similar to the one obtained in a 3-level inverter, as the nearest vertices are switched to synthesize the sample.

With this PWM strategy, the space vector combinations-11', 22', 33', 44', 55' and 66' are exclusively employed, whenever the location 'O' is switched. It is worth noting that with this PWM strategy, the location 'O' is employed as an 'active' location while the sub-hexagonal centers constitute the 'null' locations as switching is performed around them. From table-2, it may be observed that these combinations result in a zero-sequence voltage that is zero. In contrast, the PWM strategy proposed in [6] employs the location 'O' as a 'null' location. Whenever the location 'O' is switched with this PWM strategy [6], the combinations 87' and 78' are used. From table-2, it may be noted that these two combinations result in maximum zero-sequence voltages, particularly for low modulation indices wherein the dwell time associated with the 'null' vector location 'O' is more. Thus, a significant reduction in the zero-sequence voltage in the difference of pole voltages is possible with the PWM strategy proposed in this paper. For a modulation of 40%, the zero-sequence voltage resulting with the strategy adopted in [6] is about 1.4 p.u., while with the biasing inverter strategy it is 0.4 p.u. for the same modulation depth. The normalized harmonics spectra of the difference of a-phase pole voltages of the two inverters with the PWM scheme adopted in the earlier work reported [6], and using the two PWM schemes proposed in this paper i.e. Decoupled PWM scheme and Biasing Inverter PWM scheme for different modulation indices are shown in Fig.46.

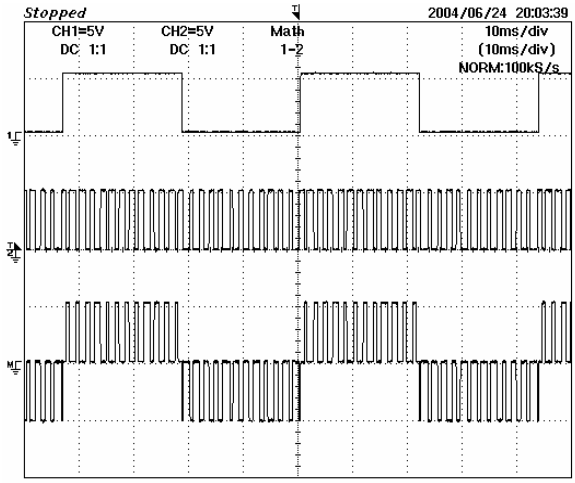

Fig.29: Gating signals and the difference of pole-voltages derived as the difference of two gate signals of top switch of the a-phase legs of the two inverters for m_i = 0.4

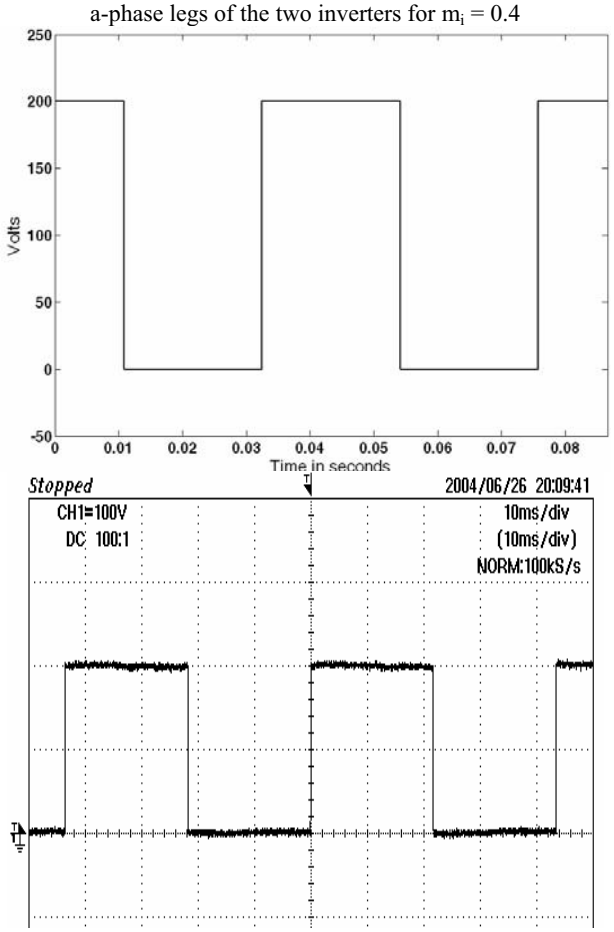

Fig.30: Simulated (top) & experimentally obtained result (bottom) of Pole voltage of inverter-1 for m_i = 0.4

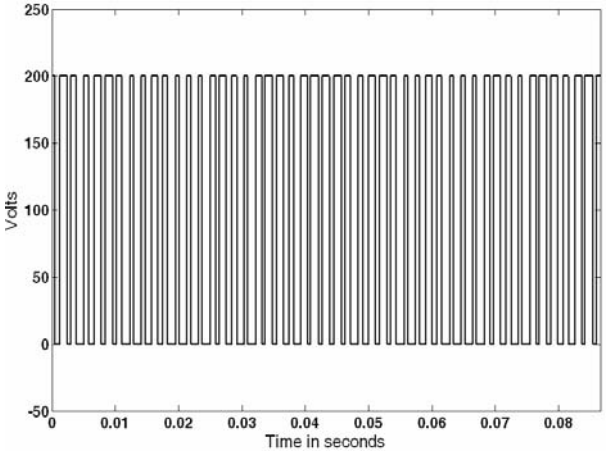

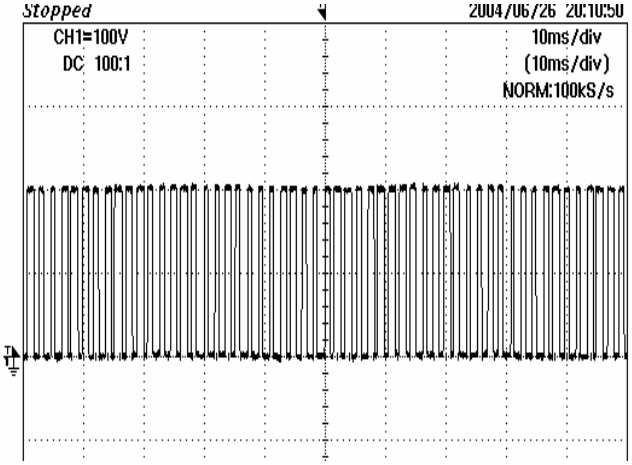

Fig.31: Simulated (top) & experimentally obtained result (bottom) of Pole voltage of inverter-2 for $m_i = 0.4$

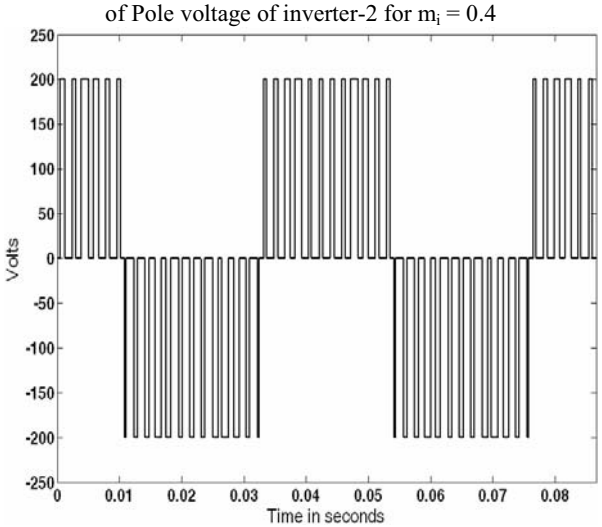

Fig.32: The difference of pole voltages of individual inverters for $m_i = 0.4$

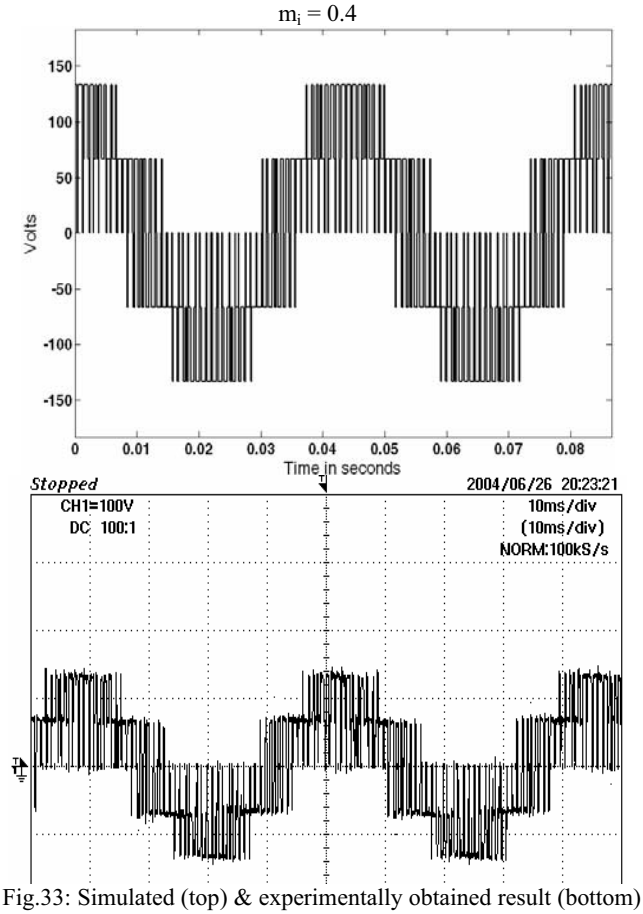

Fig.33: Simulated (top) & experimentally obtained result (bottom) of the actual motor phase voltage for $m_i = 0.4$

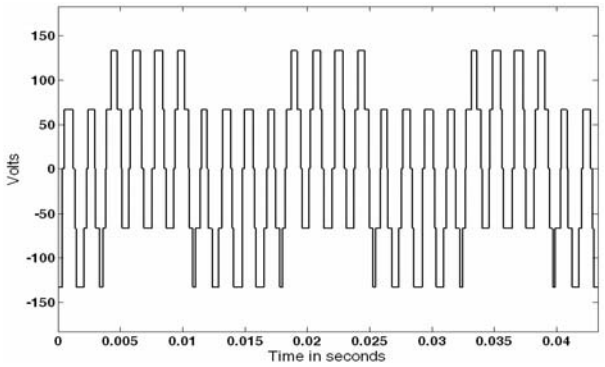

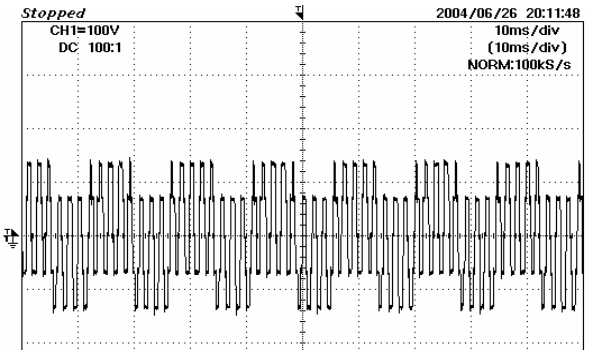

Fig.34: Simulated (top) & experimentally obtained result (bottom) of the common-mode voltage for $m_i = 0.4$

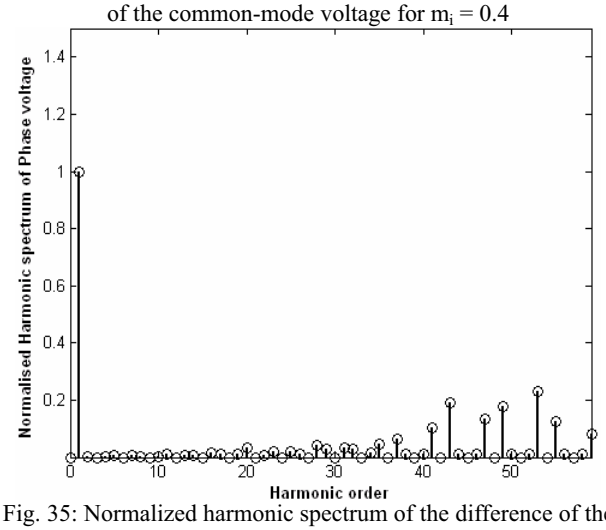

Fig. 35: Normalized harmonic spectrum of the difference of the pole voltages for $m_i = 0.4$

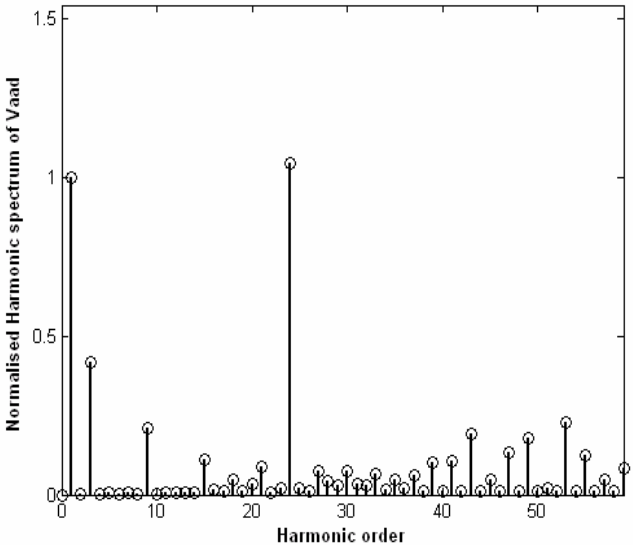

Fig. 36: Normalized harmonic spectrum of the motor phase voltage for $m_i = 0.4$

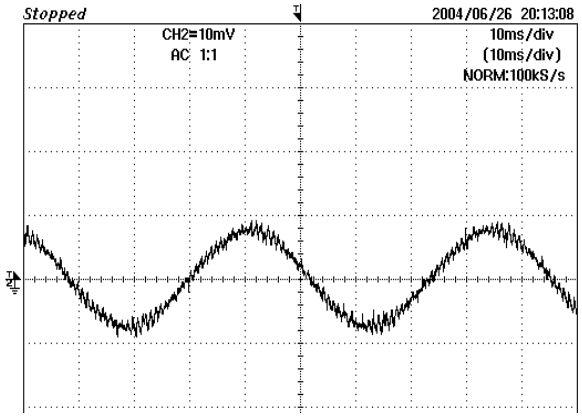

Fig.37: Experimentally obtained motor phase current at no-load for $m_i = 0.4$

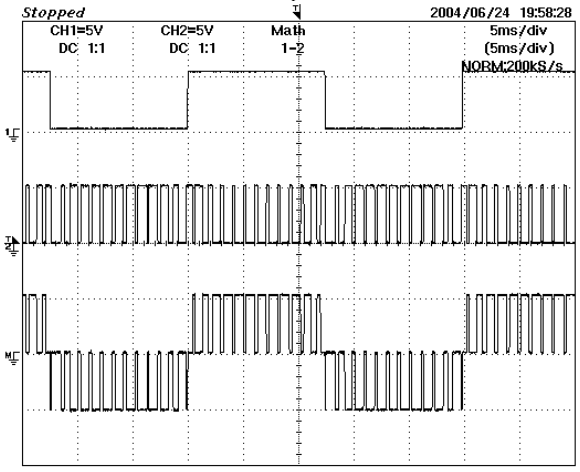

Fig.38: Gating signals and the difference of pole-voltages derived as the difference of two gate signals of top switch of the a-phase legs of the two inverters for $m_i = 0.7$

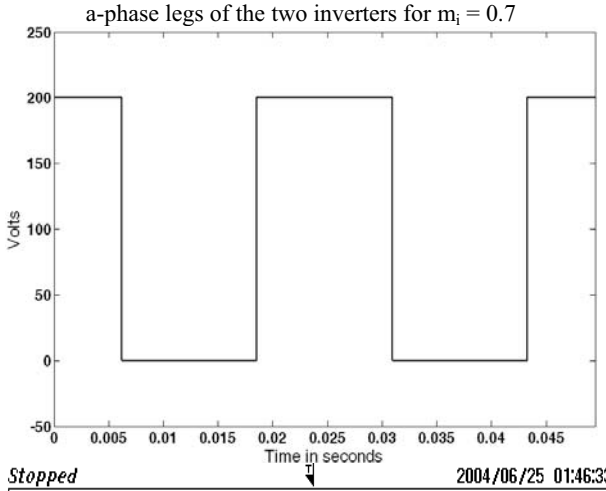

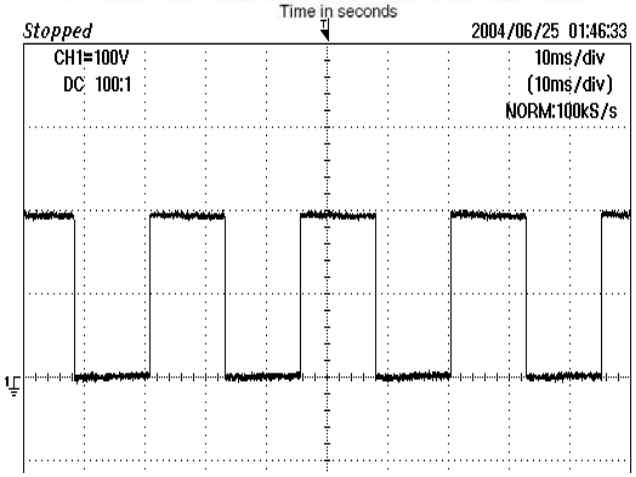

Fig.39: Simulated (top) & experimentally obtained result (bottom) of Pole voltage of inverter-1 for $m_i = 0.7$

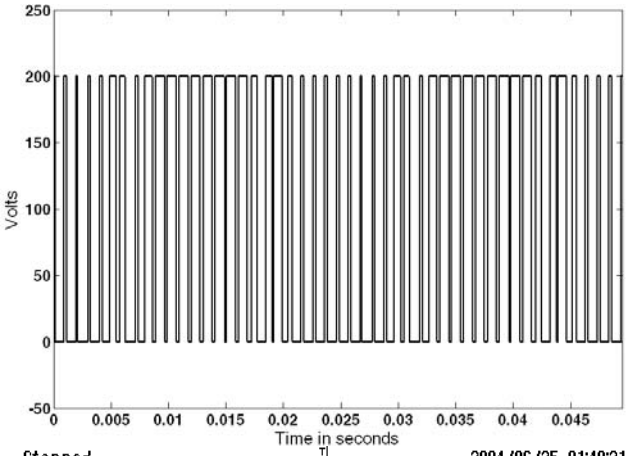

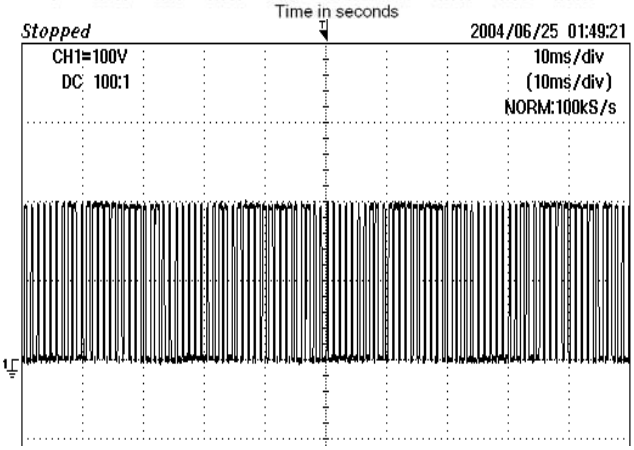

Fig.40: Simulated (top) & experimentally obtained result (bottom) of Pole voltage of inverter-2 for $m_i = 0.7$

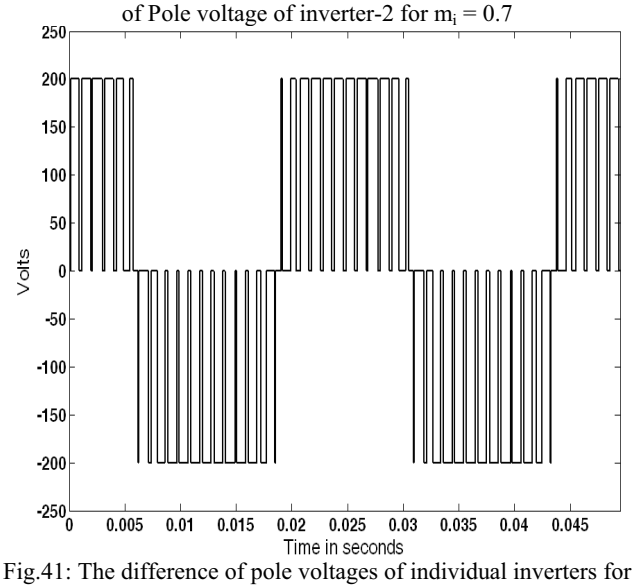

Fig.41: The difference of pole voltages of individual inverters for $m_i = 0.7$

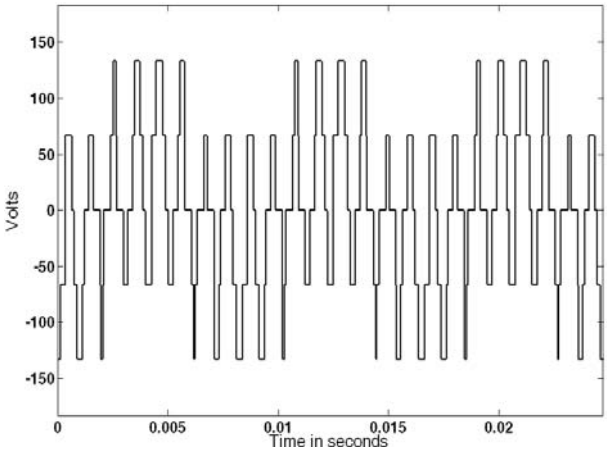

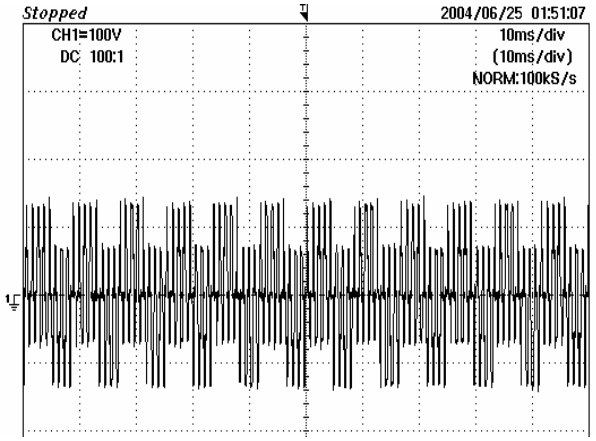

Fig.42: Simulated (top) & experimentally obtained result (bottom) of the common-mode voltage for $m_i = 0.7$

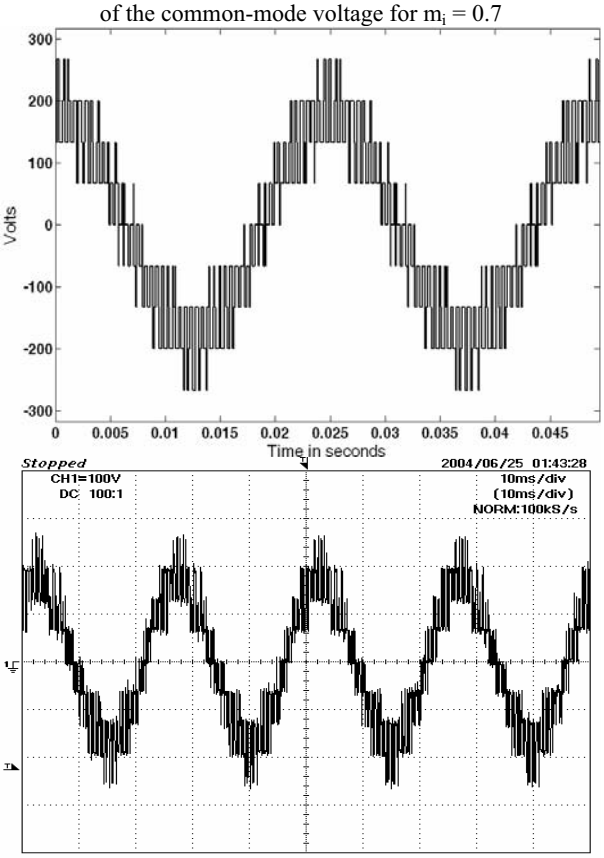

Fig.43: Simulated (top) & experimentally obtained result (bottom) of the actual motor phase voltage for $m_i = 0.7$

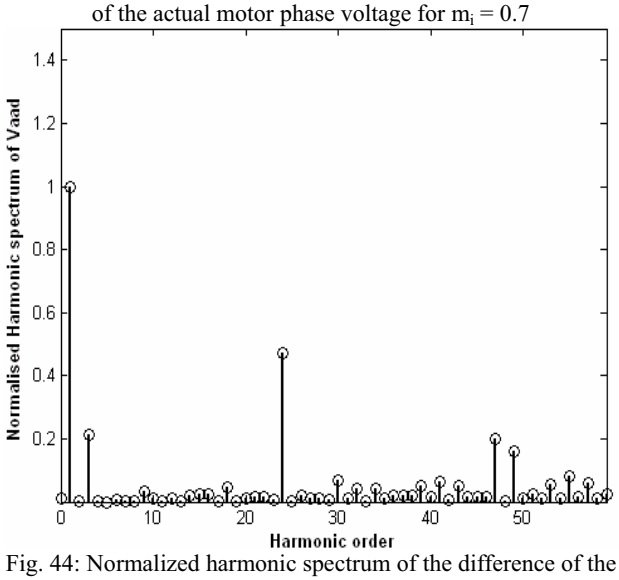

Fig. 44: Normalized harmonic spectrum of the difference of the pole voltages for $m_i = 0.7$

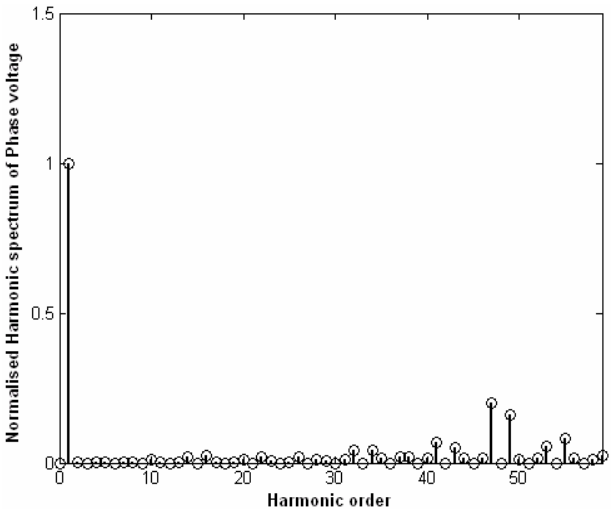

Fig. 45: Normalized harmonic spectrum of the motor phase voltage for $m_i = 0.7$

VII. Conclusions

Comparing the resultant motor phase voltages with the two PWM strategies proposed in this paper, (Fig.23 and Fig.43) it is clear that it is possible to synthesize a conventional three-level inverter waveform with the biasing inverter PWM strategy. With the biasing inverter PWM strategy the reference space vector is reproduced in the average sense by switching amongst the vector combinations available at the nearest three vertices. Consequently the switching ripple with this strategy is lesser than the decoupled PWM strategy. From the harmonic spectra of the resultant motor phase voltage with these two strategies (Fig.17 and Fig.29), it is seen that the distribution of harmonic energy is better with the biasing inverter PWM strategy. However, as pointed out earlier, the principal advantage with the decoupled PWM algorithm is its fastness and its amenability of implementation with slower controllers. It is interesting to note that the PWM strategies proposed in this paper result in a significant reduction in the zero-sequence voltage in the difference of pole-voltages compared to the look-up table approach proposed in [6] at lower indices of modulation, which could be desirable. Both strategies obviate the time consuming process of sector identification and the coordinate transformations. Look-up tables are not needed with the proposed PWM strategies, reducing the memory requirements of the controller.

References

[1] Akira Nabae, Isao Takahashi and Hirofumi Akagi, "A New Neutral-Point Clamped PWM Inverter", IEEE Trans. Ind. Appl., Vol. IA-17, No. 5, September-October 1981, pp. 518-523.

[2] T.A. Meynard and H Foch, "Multi-Level Conversion: High Voltage Choppers and Voltage Source Inverters," Conf. Proc. IEEE PESC 1992, pp. 397-403.

[3] Leon M. Tolbert, Fang Zheng Peng and Thomas G. Habetler, "Multilevel Converters for Large Electric Drives," IEEE Trans. Ind. Appl., Vol. 35, No. 1, January-February 1999, pp. 36-44.

[4] H. Stemmler, P. Guggenbach, "Configurations of High-Power Voltage Source Inverter Drives", Proceedings EPE Conference, 1993, pp. 7-14.

[5] Joohn-Sheok Kim, Seung-Ki Sul, "A Novel Voltage Modulation Technique of the Space Vector PWM", Conference Proceedings IPEC-1995, pp. 742-747.

[6] E.G. Shivakumar, K. Gopakumar, S.K. Sinha, Andre Pittet, V.T. Ranganathan, "Space Vector Control of Dual Inverter Fed Open-End Winding Induction Motor Drive", EPE Journal, Vol. 12, No. 1, February 2002, pp. 9-18.
[7] V.T. Somasekhar, K. Gopakumar, "Three-Level Inverter Configuration Cascading Two Two-Level Inverters", IEEE Proc. Electr. Power Appl., Vol. 150, No. 3, May 2003, pp. 245-254.
[8] V.T. Somasekhar, K. Gopakumar, A. Pittet and V.T. Ranganathan, "PWM Inverter Switching Strategy for a Dual Two-Level Inverter Fed Open End Winding Induction Motor Drive with a Switched Neutral", IEE Proc. Of Electr. Power Appl., Vol. 149, No, 2, March 2002, pp. 152-160.
[9] V.T. Somasekhar, K. Gopakumar, M.R. Baiju, K.K. Mohapatra and L. Umanand, "A Multilevel Inverter System for an Open End Winding Induction Motor with Open-End Windings," IEEE Transactions on Industrial Electronics, Vol. 52, No. 3, June 2005, pp. 824-836.
[10] V.T. Somasekhar, K. Gopakumar, E.G. Shivakumar, S.K. Sinha, "A Space Vector Modulation Scheme for Dual Two Level Inverter Fed an Open-End Winding Induction Motor Drive for the Elimination of Zero Sequence Current", EPE Journal, Vol. 12, No. 2, May 2002, pp. 26-36.
[11] V.T. Somasekhar, M.R. Baiju and K. Gopakumar, "Dual Two Level Inverter Scheme for an Open-End Winding Induction Motor Drive with a Single DC Power Supply and Improved DC Bus Utilization", IEE Proc. of Electr. Power. Appl., Vol. 151, No. 2, March 2004, pp. 230-238.
[12] M. B. Baiju, K.K. Mohapatra, R.S. Kanchan and K. Gopakumar, "A Dual Two-Level Inverter Scheme with Common Mode Voltage Elimination for an Induction Motor Drive", IEEE Transactions on Power Electronics. Vol. 19, No. 3, May 2004, pp. 794-805.
[13] V. Oleschuk, B.K. Bose, A.M. Stankovic, "Phase-Shift-Based Synchronous Modulation of Dual-Inverters for an Open-End Winding Induction Motor Drive with Elimination of Zero Sequence Currents", Conf. Proc. IEEE-PEDS-2005, pp. 325-330.
[14] V. Oleschuk, F. Profumo, A. Tenconi and R. Bojoi, "Synchronized Pulse_Width Modulation for Control of Inverter-Fed Open-End Winding Motor Drives", EPE Conf. Proc., Pelincec, 2005, Paper-ID: 94.

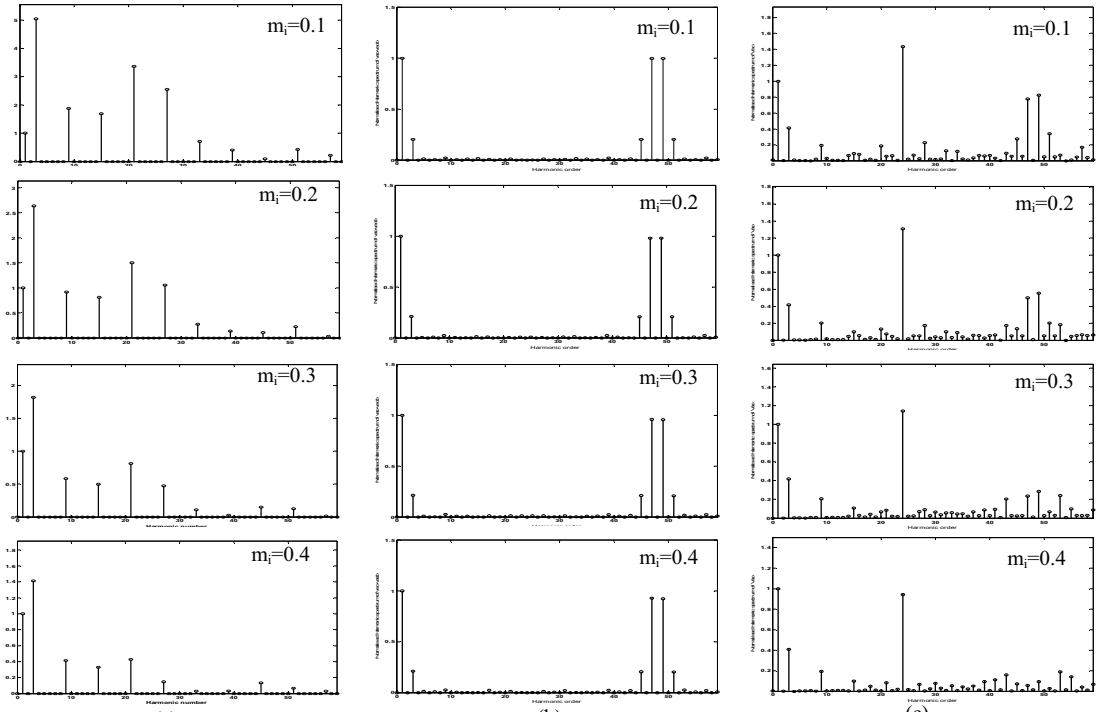

(a) (b) (c)

APPENDIX

The imaginary switching times [5] for inverter-1 and inverter-2 are related to the respective phase reference voltages as follows:

$$T_{as} = 2(\frac{T_s}{V_{dc}})v_a^* \quad (1)$$

$$T_{bs} = 2(\frac{T_s}{V_{dc}})v_b^* \quad (2)$$

$$T_{cs} = 2(\frac{T_s}{V_{dc}})v_c^* \quad (3)$$

$$T_{ga}^{'} = -2(\frac{T_s}{V_{dc}})v_a^* \quad (4)$$

$$T_{gb}^{'} = -2(\frac{T_s}{V_{dc}})v_c^* \quad (5)$$

$$T_{gc}^{'} = -2(\frac{T_s}{V_{dc}})v_c^* \quad (6)$$

When the reference vector is situated in sector-1,
For Inverter-1:

$$T_{\max} = T_{as}$$

$$T_{\min} = T_{CS}$$

$$As\ T_{eff} = T_{\max} - T_{\min}[5]$$

$$\Rightarrow T_{eff} = T_{as} - T_{cs}$$

Using equations (1), (2) & (3), we have

$$T_{eff} = 2(\frac{T_s}{V_{dc}})(v_a^* - v_c^*) \quad (7)$$

Similarly for Invertre-2:

$$T_{\min}^{'} = T_{as}^{'}$$

$$T_{\max}^{'} = T_{cs}^{'}$$

$$\therefore T_{eff}^{'} = T_{cs}^{'} - T_{as}^{'}$$

Using equations (4), (5) & (6), we have

$$T_{eff}^{'} = 2(\frac{T_s}{V_{dc}})(v_a^* - v_c^*) \quad (8)$$

It is obvious that the effective-time period for inverter-1 and inverter-2 are equal, as the reference vector is resolved into two equal halves.

From equations (7) & (8), we have

$$T_{eff} = T_{eff}^{'} \quad (9)$$

As $T_o = T_s - T_{eff}$ & $T_o^{'} = T_s - T_{eff}^{'}$ *[5]*

$\Rightarrow T_o = T_o^{'}$ *[from eqn.(9)]*

It was shown in [5] that the time-offset required to place the effective time period at the centre of the sampling time interval is given by:

$$T_{offset} = \frac{T_o}{2} - T_{\min}$$

Hence for inverter-1, the time-offset is:

$$T_{offset} = \frac{T_o}{2} - 2(\frac{T_s}{V_{dc}})v_c^*$$

$$T_{offset}^{'} = \frac{T_o}{2} - T_{\min}^{'}$$

Similarly,

$$= \frac{T_o}{2} + 2(\frac{T_s}{V_{dc}})v_a^*$$

From the algorithm proposed in [5], the phase switching time for phase-A for inverter-1 is given by:

$$T_{ga} = T_{as} + T_{offset} \quad (10)$$

$$= 2(\frac{T_s}{V_{dc}})v_a^* + \frac{T_o}{2} - 2(\frac{T_s}{V_{dc}})v_c^*$$

$$\therefore T_{ga} = \frac{T_o}{2} + 2(\frac{T_s}{V_{dc}})(v_a^* - v_c^*) \quad (11)$$

Similarly for inverter-2,

$$T_{ga}^{'} = T_{as}^{'} + T_{offset}^{'}$$

$$= -2(\frac{T_s}{V_{dc}})v_a^* + \frac{T_o}{2} + 2(\frac{T_s}{V_{dc}})v_a^*$$

$$\therefore T_{ga}^{'} = \frac{T_o}{2} \quad (12)$$

From equations (11) & (12), it is evident that

$$T_{ga} + T_{ga}^{'} = T_o + 2(\frac{T_s}{V_{dc}})(v_a^* - v_c^*)$$

From eqn.7, $T_{ga} + T_{ga}^{'} = T_o + T_{eff} = T_s$

$\therefore T_{ga}^{'} = T_s - T_{ga}$

Similarly, the phase switching times for the other two phases are given as:

$\therefore T_{gb}^{'} = T_s - T_{gb}$

$\therefore T_{gc}^{'} = T_s - T_{gc}$

BIOGRAPHIES

S.Srinivas received the B.E degree in Electrical Engineering from Osmania University College of Engineering and his Masters degree from Regional Engineering College-Warangal in 1997 and 2002 respectively.

He is currently working towards the Ph.D degree at National Institute of Technology-Warangal.

He joined the Faculty of Electrical Engineering National Institute of Technology-Warangal in the year 1997. His research interests are multi-level inverters, PWM Switching Strategies, Multi-level inversion realized through Open-end winding Induction motor drives, AC drives etc.

Dr. V.T. Somasekhar received his graduate degree from Regional Engineering College Warangal (presently the National Institute of Technology) in 1988 and the post graduate degree from the Indian Institute of Technology, Bombay in 1990, his area of specialization being Power Electronics. He worked as an R&D engineer at M/s Perpetual Power Technologies, Bangalore and as a senior engineer at M/s Kirloskar Electric Co. Ltd., Mysore. He joined the faculty of electrical engineering at the National Institute of Technology in 1993, where he is currently serving. He received his doctoral degree from the Indian Institute of Science in 2003. His current interests are multilevel inversion with open-end induction motors, AC drives and PWM strategies.